THE JOURNAL OF BIOLOGICAL CHEMISTRY
Vol. 275, No. 48, Issue of December 1, pp. 37807–37814, 2000

Printed in U.S.A.

Synaptic Localization and Presynaptic Function of Calcium Channel β_4-Subunits in Cultured Hippocampal Neurons*

Received for publication, May 30, 2000, and in revised form, August 1, 2000
Published, JBC Papers in Press, August 7, 2000, DOI 10.1074/jbc.M004653200

Silke Wittemann‡, Melanie D. Mark‡, Jens Rettig§, and Stefan Herlitze‡¶

From the ‡Department of Physiology II, University of Tuebingen, Ob dem Himmelreich 7, 72074 Tuebingen, Germany and the §Department of Membrane Biophysics, Max-Planck-Institute for Biophysical Chemistry, Am Fassberg 11, 37077 Goettingen, Germany

Neurotransmitter release is triggered by the influx of Ca^{2+} into the presynaptic terminal through voltage gated Ca^{2+}-channels. The shape of the presynaptic Ca^{2+} signal largely determines the amount of released quanta and thus the size of the synaptic response. Ca^{2+}-channel function is modulated in particular by the auxiliary β-subunits that interact intracellularly with the pore-forming α_1-subunit. Using retrovirus-mediated gene transfer in cultured hippocampal neurons, we demonstrate that functional GFP-β_4 constructs colocalize with the synaptic vesicle marker synaptobrevin II and endogenous P/Q-type channels, indicating that β_4-subunits are localized to synaptic sites. Costaining with the dendritic marker MAP2 revealed that the β_4-subunit is transported to dendrites as well as axons. The nonconserved amino- and carboxyl-termini of the β_4-subunit were found to target the protein to the synapse. Physiological measurements in autaptic hippocampal neurons infected with green fluorescent protein (GFP)-β_4 revealed an increase in both excitatory post-synaptic current amplitude and paired pulse facilitation ratio, whereas the GFP-β_4 mutant, GFP-β_4(Δ50–407), which demonstrated a cytosolic localization pattern, did not alter these synaptic properties. In summary, our data suggest a presynaptic function of the Ca^{2+}-channel β_4-subunit in synaptic transmission.

Ca^{2+}-channels mediate voltage-dependent Ca^{2+}-influx in subcellular compartments of neurons, triggering such diverse processes as neurotransmitter release and excitation-transcription coupling (1, 2). Neuronal Ca^{2+}-channels consist of a pore-forming α_1-subunit and several auxiliary subunits (β-, $\alpha_2\delta$-, and presumably γ-subunits), which are associated with the α_1-subunit. Ca^{2+}-channel function is determined by different β-subunits, which modify the gating properties of the channel and most likely the transport of the α_1-subunit to the cell surface (3–7). Expression of the four different β-subunits has been shown in various brain regions such as the cerebellum and hippocampus. Here, β-subunits were expressed in neuronal cell bodies, dendrites, and neuropils (8–11). A pre- and post-synaptic localization has been suggested for β_1-, β_3-, and β_4-subunits, but a precise role for any β-subunit in synaptic transmission has not been described so far.

New approaches in cell biology to study protein targeting within a cell, *e.g.* GFP[1] and viral transfection methods, allow the overexpression of ion channel subunits in cultured neuronal cells to analyze their transport to specific subcellular compartments (12). Applying these methods, we investigated the distribution and specific function of the Ca^{2+}-channel β_4-subunit in cultured hippocampal neurons. We demonstrated that the β_4-subunit is localized to presynaptic terminals and that its N and C termini are responsible for this specific targeting. Furthermore, we show that β_4-subunits of voltage-gated Ca^{2+}-channels play an important physiological role in synaptic transmission by altering amplitude and activity-dependent properties of the synaptic response.

EXPERIMENTAL PROCEDURES

Construction of GFP Fusion Proteins and Deletion Mutants—The rat β_4 cDNA (13) was amplified with the following primer pairs, which include restriction sites for subcloning: 5′-GATCTCGAGATGTCGTCCTCCTACGCCAAG and 3′-ACGGTCGACTCAAAGCCTATGTCGGGAGTC.

The constructs were subcloned in-frame into pEGFP-C_3 (CLONTECH) and then excised for cloning into the Semliki Forest virus vector pSFV1 (Life Technologies, Inc.). Deletion mutants were constructed using a single PCR reaction where restriction sites for subcloning into pEGFP-C_3 (CLONTECH) were placed within the oligonucleotide primer. The following primer pairs were used for the deletion mutants: N terminus (aa 1–49), 5′-GATCTCGAGATGTCGTCCTCCTACGCCAAG and 3′-GGGGGATCCCCCCTGTCTGAGGATGAAGCTGGT; C terminus (aa 408–519), 5′-CCCAAGCTTCCTATGACCCCATTGCTGGGG and 3′-ACGGTCGACTCAAAGCCTATGTCGGGAGTC; Δ50–407, 5′-GATCTCGAGTCAGCAGATTCCTATACA and 3′-CCCAAGCTTGGTGCTACTGCTTGTGTGGGT.

The pEGFP-C_3-β_4 deletion clones were subcloned into pSFV by blunt end cloning and correct orientation of the constructs were verified by cDNA sequencing. cDNAs encoding β_4 (13), GFP-β_4, and GFP-β_4(Δ50–407) in pEGFP-C_3 (CLONTECH) were used for whole cell recordings. Western blotting of infected HEK293 cells with a monoclonal anti-GFP antibody (CLONTECH) was performed according to standard procedures as described by Mark *et al.* (14).

Cell Culture and Electrophysiology—HEK293 cells were transfected with the Ca^{2+}-channel subunits α_{1A}, $\alpha_2\delta$, and β_4, GFP-β_4, or GFP-β_4(Δ50–407). cDNAs and whole cell recordings were performed as published previously (15). Membrane capacitance and series resistance were compensated electronically using the patch clamp amplifier (EPC-9; HEKA, Lambrecht, Germany). Voltage protocol design and data acquisition were performed using Pulse++, version 1.7 software (Ulix GmbH, Tuebingen, Germany) on a Macintosh Power PC. Inactivation measurements for control of functional GFP constructs (Figs. 1 and 5) were performed with 10 mM Ba^{2+} as the current carrier at room temperature. 2- and 10-ms inactivation protocols were measured with 4 mM Ca^{2+} instead of Ba^{2+} as the current carrier, also at room temperature (extracellular solution in mM: 100 Tris, 4 $MgCl_2$, 4 $CaCl_2$, pH 7.3, with methanesulfonic acid). Ca^{2+}- and Ba^{2+}-currents were analyzed

* This work was supported by grants from the Deutsche Forschungsgemeinschaft (He2471/5-1 to S. H. and Re1092/3-2 to J. R.). The costs of publication of this article were defrayed in part by the payment of page charges. This article must therefore be hereby marked "*advertisement*" in accordance with 18 U.S.C. Section 1734 solely to indicate this fact.

¶ To whom correspondence should be addressed. Tel.: 049-7071-2978279; Fax: 049-7071-87815; E-mail: stefan.herlitze@uni-tuebingen.de.

[1] The abbreviations used are: GFP, green fluorescent protein; aa, amino acid(s); EPSC, excitatory post-synaptic current; HEK, human embryonic kidney.

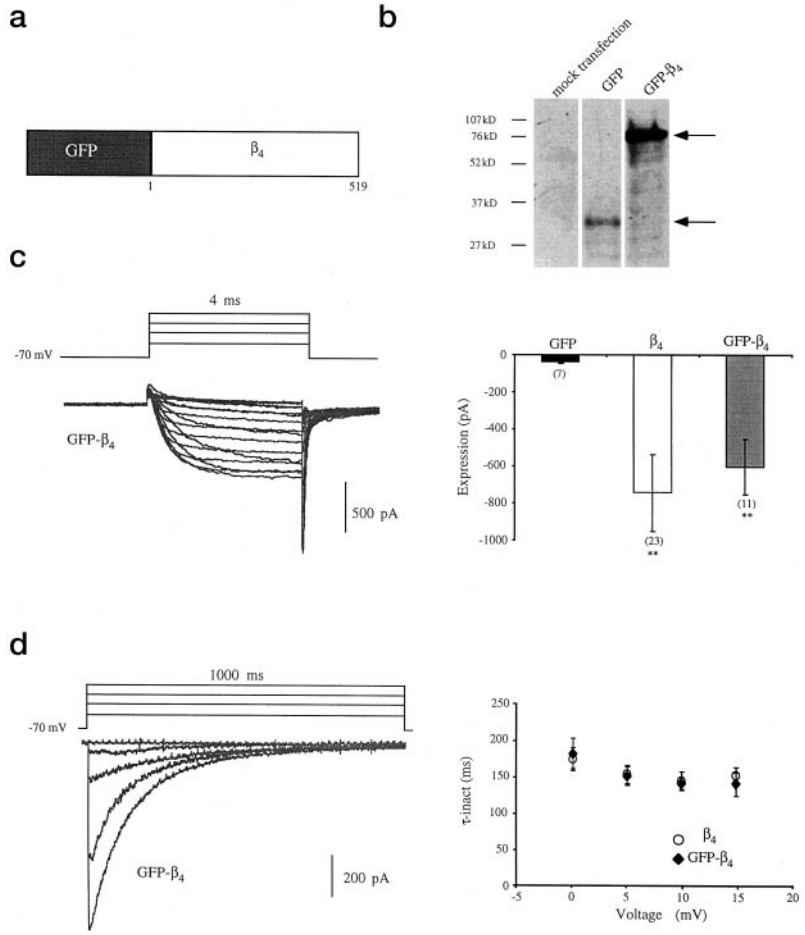

FIG. 1. **Western blot analysis and whole cell recordings of HEK293 cells expressing GFP-β_4.** *a*, schematic representation of the GFP-β_4 fusion construct used in the experiments described. GFP was tagged in-frame to the N terminus of β_4. The β_4-subunit consists of 519 aa. *b*, Western blot analysis of GFP and GFP-β_4 expressed in HEK293 cells. Proteins were detected with a monoclonal antibody against GFP. Purified GFP-β_4 protein shows the expected size of 83 kDa. *c*, whole cell recordings of HEK293 cells co-transfected with the α_{1A}, $\alpha_2\delta$, and GFP-β_4 or wild-type-β_4. *Left*, representative Ba^{2+}-currents from an α_{1A}, $\alpha_2\delta$, and GFP-β_4 assembled channels were elicited by 4-ms, 5-mV step potentials from −50 to +50 mV from a holding potential of −70 mV. *Right*, Ba^{2+}-currents were measured at +10 mV during the 500-ms voltage ramps. *Bars* represent cells transfected with the following DNAs: *black bar,* α_{1A}, $\alpha_2\delta$, and GFP; *white bar*, α_{1A}, $\alpha_2\delta$, wild-type-β_4, and GFP; *gray bar*, α_{1A}, $\alpha_2\delta$, and GFP-β_4. The Ba^{2+}-currents are significantly larger for cells expressing the β_4-subunit ($p > 0.01$, two-tailed *t* test) but are not significantly different between wild-typeβ_4 and GFP-β_4. *d, left*, representative traces of Ba^{2+}-currents from α_{1A}, $\alpha_2\delta$, and GFP-β_4 assembled channels elicited by a 1000-ms test pulse to −50, 0, +5, +10, and +15 mV from a holding potential of −70 mV. *Right*, time constants for inactivation curves (τ-inact in ms) measured at 0, +5, +10, and +15 mV. Values for α_{1A}, $\alpha_2\delta$, and wild-type β_4 (*open circles*) or GFP-β_4 (*filled diamonds*) are not significantly different.

using the IGOR data analysis package (WaveMetrics, Lake Oswego, OR). Peak currents were determined from the current measured at +10 mV. Currents were elicited by a 500-ms voltage ramp from −70 mV to +50 mV. Time constants of inactivation (τ-inact) were determined by fitting the decay phase of a 1000-ms test pulse from −70 mV to +10 mV with a single exponential or, as shown in Fig. 9, by fitting the decreasing tail currents elicited by 2- or 10-ms test pulses from −70 mV to +10 mV every 50 ms with a single exponential. The percent current reduction was determined by comparing the size of the first elicited tail current and the last elicited tail current with the 20 Hz stimulation protocol. 20 test pulses were applied within the 20 Hz stimulation protocol in HEK293 cells. Statistical significance was expressed as ** $p < 0.01$. All error values (±) and bars in this publication are S.E.s.

Micro-island cultures of hippocampal neurons were prepared according to a modified version of published procedures (16). After 9–14 days in culture, cells were infected with 50 μl of an activated Semliki Forest virus containing the cDNAs of GFP-β_4 or GFP-β_4-deletion constructs following a protocol given in Ashery *et al.* (17). All measurements were performed 6–18 h after infection. Only dots containing a single neuron forming excitatory synapses (autapses) were used. Extracellular recording solution contained (in mM): 172 NaCl, 2.4 KCl, 10 HEPES, 10 glucose, 4 $CaCl_2$, 4 $MgCl_2$, and 0.03 $CdCl_2$ (pH 7.3, 350 mosmol). Patch pipettes (2–3 megaohms) were pulled from borosilicate glass (TWF 150, World Precision Instruments) on a Sutter puller and back-filled with the following (in mM): 145 potassium gluconate, 15 HEPES, 1 potassium-EGTA, 4 Na-ATP, 0.4 Na-GTP (pH 7.3). Currents were recorded and analyzed as published previously by Lao *et al.* (18).

Immunocytochemistry—Continental hippocampal cultures were prepared and infected as described above and fixed as described by Mark *et al.* (14). Neurons were incubated with synaptobrevin II antibody (C69.1 at 1:1000, a gift from R. Jahn, Göttingen, Germany), Ca^{2+}-channel α_{1A}-subunit antibody (Chemicon; 1:60) or MAP2 antibody (Sigma; 1:1000) and then with an Alexa 546-coupled secondary antibody (Molecular Probes, Leiden, Netherlands). Cells were embedded in Fluoromount (133 mM Tris-HCl, 30% glycerol, 11% Mowiol, 2% diazabicyclo(2.2.2)octane. Fluorescence was detected with a conventional fluorescence microscope (Axiophot; Carl Zeiss, Oberkochen, Germany), and images were analyzed with the Metamorph imaging system.

RESULTS

A fusion construct between GFP and the β_4-subunit was generated to analyze the distribution and function of this Ca^{2+}-channel subunit (Fig. 1*a*). The GFP was tagged in frame to the N terminus of the β_4-subunit using the mammalian expression vector pEGFP-C_3 and subcloned into the Semliki Forest virus vector (pSFV). We first investigated whether the fusion construct of the virus expresses a protein of the correct size. Western blot analysis of HEK293 cells infected with GFP-β_4 revealed an 83-kDa band, the predicted size of the GFP-β_4 fusion protein (Fig. 1*b*). In addition, the GFP-β_4 protein assembled with the α_{1A}- and $\alpha_2\delta$-subunits to form a functional voltage-gated Ca^{2+}-channel in HEK293 cells. Whole cell peak currents were measured at +10 mV during a 500-ms voltage ramp from −70 to +50 mV and increased from −38 ± 14 pA ($n = 7$) for $\alpha_{1A}/\alpha_2\delta$ to −602 ± 314 pA ($n = 11$) with the GFP-β_4 fusion protein, which was comparable to the wild-type β_4 currents (-744 ± 209 pA ($n = 23$)) (Fig. 1*c*). In addition, GFP-β_4 revealed the characteristic slow inactivation time constants at 0, +5, +10, and +15 mV (τ-inact) as described for wild-type β_4-subunit assembled with P/Q-type Ca^{2+}-channels (188 ± 22 (0 mV), 145 ± 18 (+5 mV), 131 ± 18 (+10 mV), and 130 ± 15 ms (+15 mV) ($n = 6$) for wild-type-β_4; (178 ± 29 (0 mV), 149 ± 18 (+5 mV), 136 ± 12 (+10 mV), and 147 ± 22 ms (+15 mV) ($n = 6$) for GFP-β_4) (Fig. 1*d*) (19). Thus, GFP-β_4 constructs yield functional β_4-protein, which alters the electrophysiological characteristics of the P/Q-type Ca^{2+}-channels in the expected manner.

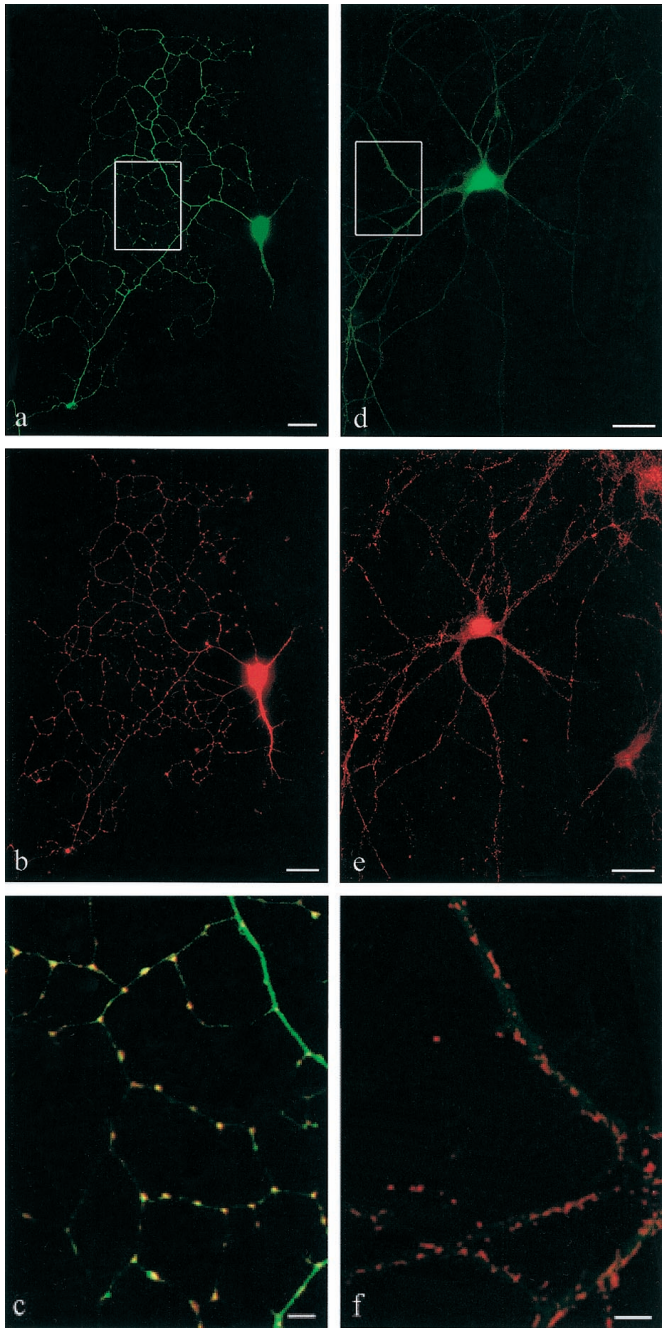

FIG. 2. **Colocalization of GFP-β_4 with synaptobrevin II in cultured hippocampal neurons.** *a*, fluorescence patterns of neurons from low density hippocampal cultures infected with GFP-β_4 reveal a punctate staining. *b*, hippocampal cells were stained with an anti-synaptobrevin II antibody and visualized with an Alexa 546-coupled secondary antibody. A punctate staining pattern similar to that seen with GFP-β_4 was observed. *c*, overlay of *a* and *b* in the indicated area demonstrates that GFP-β_4 is partially colocalized with the synaptic vesicle marker synaptobrevin II (*yellow*). *d*, fluorescence pattern of neurons from low density hippocampal cultures infected with GFP alone demonstrates a diffuse, cytosolic staining. *e*, hippocampal cells were stained with an anti-synaptobrevin II antibody and visualized with an Alexa 546-coupled secondary antibody. *f*, overlay of *d* and *e* in the indicated area demonstrates that GFP is not colocalized with the synaptic vesicle marker synaptobrevin II (*yellow*). *Scale bars* in *a, b, d*, and *e* =10 μm and in *c* and *f* = 2 μm.

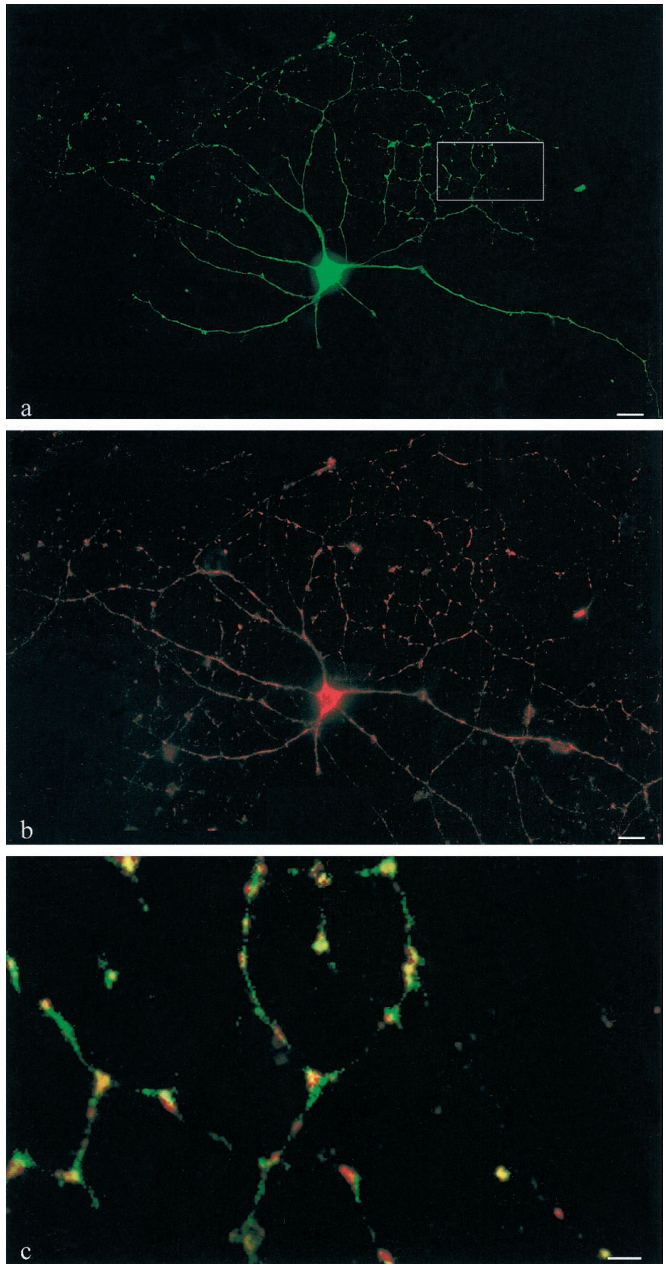

FIG. 3. **Colocalization of GFP-β_4 with Ca^{2+}-channel α_{1A}-subunit in cultured hippocampal neurons.** *a*, fluorescence patterns of neurons from low density hippocampal cultures infected with GFP-β_4 reveal a punctate staining. *b*, hippocampal cells were stained with an anti-α_{1A} antibody and visualized with an Alexa 546-coupled secondary antibody. A punctate staining pattern similar to that seen with GFP-β_4 was observed. *c*, overlay of *a* and *b* in the indicated area demonstrates that GFP-β_4 is partially colocalized with the presynaptic P/Q-type Ca^{2+}-channel subunit α_{1A} (*yellow*). *Scale bars* in *a* and *b* = 10 μm and in *c* = 5 μm.

To investigate the distribution of β_4 in hippocampal neurons, 9–14-day-old neurons were infected with the GFP-β_4 construct using the Semliki Forest virus gene expression system. Overexpressed GFP-β_4-subunits displayed a punctate staining pattern along the neuronal processes (Fig. 2, *a–c*), as observed for vesicle-transported proteins like synaptobrevin II, syntaxin, or syntaphilin, whereas overexpressed GFP alone showed a diffuse, cytosolic distribution along the neurites (Fig. 2, *d–f*). Colocalization with the synaptic vesicle marker synaptobrevin II (Fig. 2c) revealed that GFP-β_4 was indeed transported to synaptic sites. P/Q-type Ca^{2+}-channels are highly expressed in presynaptic terminals (20) and play a fundamental role in synaptic transmission (2). Because β_4-subunits can assemble with α_{1A}-subunits to form functional channels in HEK293 cells (Fig. 1), we investigated whether β_4-subunits colocalize with endogenous presynaptic Ca^{2+}-channels in hippocampal neurons. Costaining between the α_{1A}-subunit encoding for the

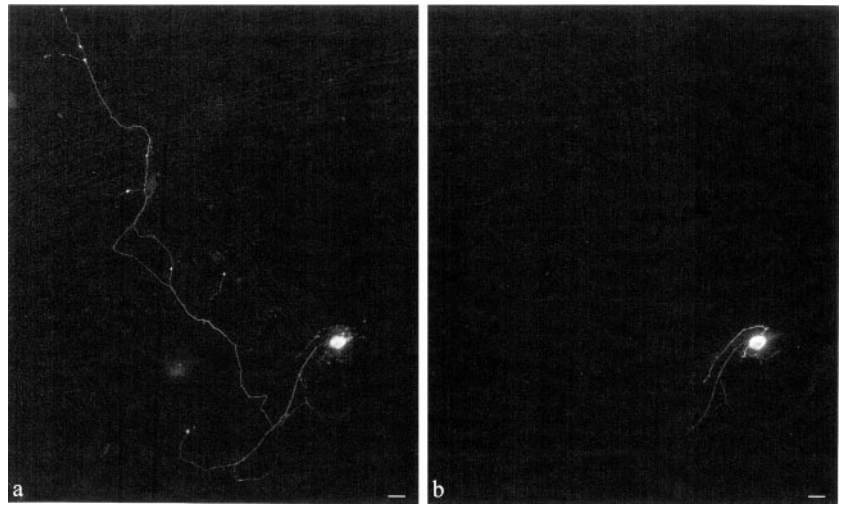

FIG. 4. **Localization of GFP-β_4 and MAP2 in cultured hippocampal neurons.** *a*, fluorescence patterns of neurons from low density hippocampal cultures infected with GFP-β_4 reveal staining in dendrites and axons. *b*, hippocampal cells were stained with an anti-MAP2 antibody and visualized with an Alexa 546-coupled secondary antibody. MAP2 stains only the dendrites and not the axon. Scale bars = 10 μm.

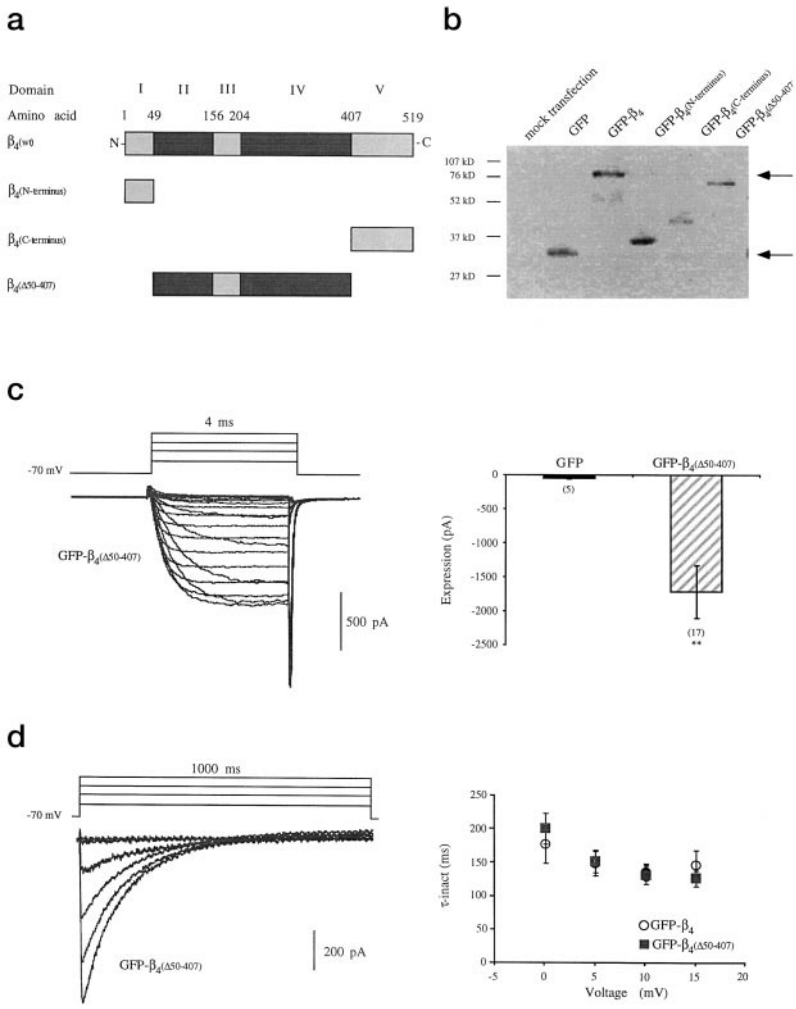

FIG. 5. **GFP-β_4 deletion constructs.** *a*, schematic representation of β_4 domain structure and derived deletion constructs. The β-subunit is divided into 5 domains (**I**, **II**, **III**, **IV**, **V**). The *black bars* represent the domains with a high degree of conservation between all four β-subunit isoforms (β_{1b}, β_3, β_{2a}, and β_4), and the *gray bars* represent domains with a low degree of conservation (22, 41). *b*, Western blot analysis of GFP and GFP-β_4 deletion constructs expressed in HEK293 cells. Proteins were detected as described in Fig. 1*b* legend. *c*, whole cell recordings of HEK293 cells cotransfected with α_{1A}, $\alpha_2\delta$, and with or without GFP-β_4(Δ50–407). *Left*, representative Ba^{2+}-currents from α_{1A}, $\alpha_2\delta$, and GFP-β_4(Δ50–407) assembled channels were elicited by 4-ms, 5-mV step potentials from −50 to +50 mV from a holding potential of −70 mV. *Right*, Ba^{2+}-currents were measured at +10 mV during 500-ms voltage ramps. *Bars* represent cells transfected with the following DNAs: *black bar*, α_{1A}, $\alpha_2\delta$, and GFP; *striped bar*, α_{1A}, $\alpha_2\delta$, and GFP-β_4(Δ50–407). The Ba^{2+}-currents are significantly larger for cells expressing the GFP-β_4(Δ50–407) construct ($p > 0.01$, two-tailed *t* test). *d, left*, representative traces of a Ba^{2+}-currents from α_{1A}, $\alpha_2\delta$, and GFP-β_4(Δ50–407) assembled channels elicited by a 1000-ms test pulse to −50, 0, +5, +10, and +15 mV from a holding potential of −70 mV. *Right*, time constants for inactivation curves (τ-inact in ms) measured at 0, +5, +10, and +15 mV. Values for Ca^{2+}-channels assembled with the GFP-β_4 (*open circles*) or GFP-β_4(Δ50–407) (*filled squares*) are not significantly different.

P/Q-type channel and GFP-β_4 demonstrated the colocalization of both proteins (Fig. 3). Next, we investigated whether the β_4-subunit is localized to dendrites or axons. Double-labeling with the dendritic marker MAP2 identified the fact that GFP-β_4 is transported to both dendrites and axons (Fig. 4). Thus, our results highly suggest that the β_4-subunit is targeted to synaptic sites.

Based on the sequence alignment, the predicted structure of β_{1b}-subunit, and functional analysis, β-subunits can be divided into five domains (21, 22) (Fig. 5*a*). A high degree of conservation among the β-subunits was observed for domains **II** and **IV**, but not for domains **I** (N terminus), **III**, and **V** (C terminus). To determine which domain of β_4 is responsible for targeting this subunit to its specific subcellular localization, we produced several deletion constructs of GFP-β_4 according to the domain assignment (Fig. 5*a*). These constructs expressed fusion proteins of the expected size (Fig. 5*b*). The minimal segments required for punctate localization and colocalization with syn-

TABLE I

Statistical analysis of punctate staining pattern in hippocampal neurons infected with various β_4 constructs

Low density hippocampal cultures were prepared and infected with various β_4 constructs after 9–14 days in culture, fixed, and analyzed as described under "Experimental Procedures."

Infected constructs	Number of infected cells with punctate staining	Number of infected cells with no punctate staining	Percentage of infected cells with punctate staining (%)	No. of cells analyzed
GFP-β_4	220	17	93	237
GFP-C-terminus	198	7	97	205
GFP-N-terminus	143	57	72	200
GFP-$\beta_{4(\Delta 50-407)}$	59	154	28	213
GFP	19	176	11	195

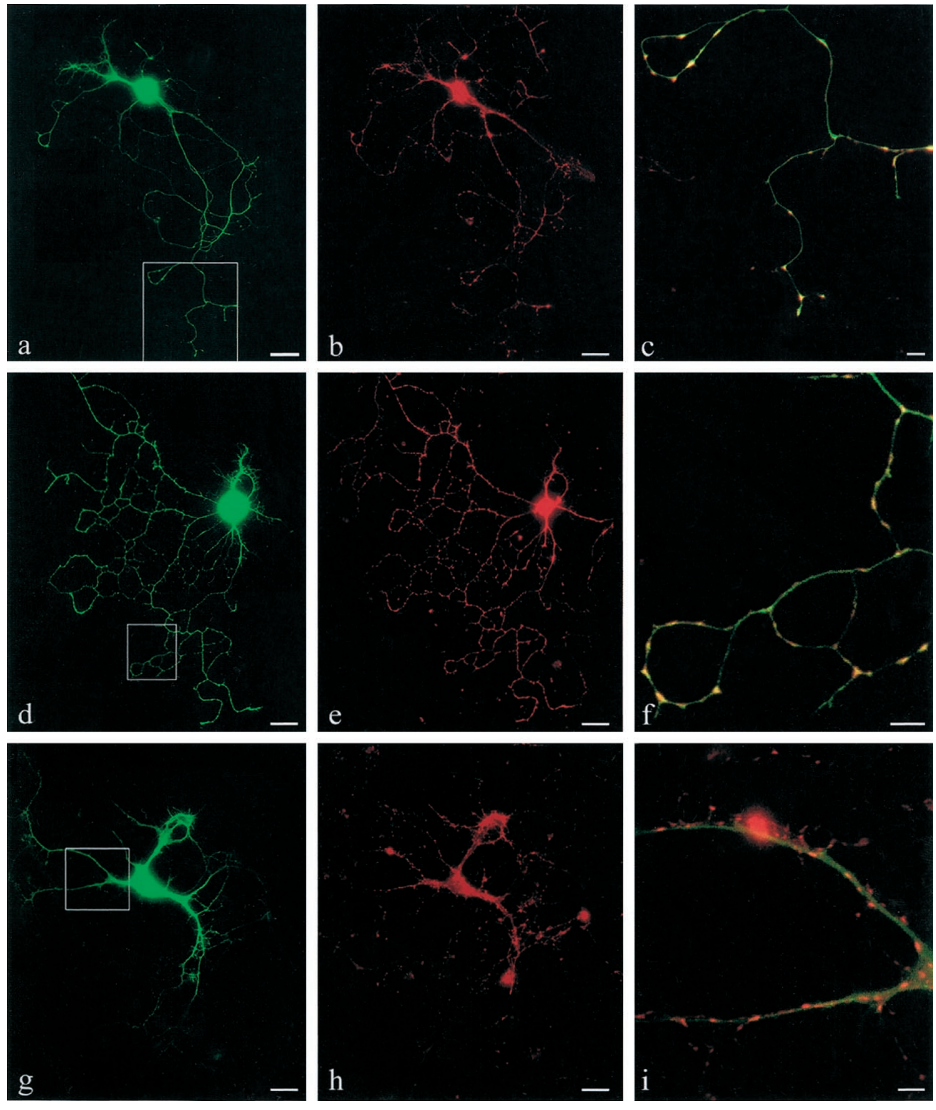

FIG. 6. **Distribution and colocalization of GFP-β_4 deletion constructs with synaptobrevin II in cultured hippocampal neurons.** *a, d,* and *g*, fluorescence patterns of neurons from low density hippocampal cultures infected with GFP-β_4 deletion constructs (*a*, N terminus; *d*, C terminus; *g*, GFP-β_4(Δ50–407)). *b, e,* and *h*, hippocampal cells were stained with an anti-synaptobrevin II antibody and visualized with an Alexa546-coupled secondary antibody. *c, f,* and *i*, overlays of *a* and *b* (N terminus), *d* and *e* (C terminus), and *g* and *h* (GFP-β_4(Δ50–407)) demonstrate that GFP-β_4-N terminus and GFP-β_4-C terminus (domains **I** and **V**), but not GFP-β_4(Δ50–407), are colocalized with the synaptic vesicle marker synaptobrevin II (*yellow*). *Scale bars* = 10 μm for *a*, *b*, *d*, *e*, *g*, and *h* and 2 μM for *c*, *f*, and *i*.

aptobrevin II were domain **I** (N terminus, aa 1–49) and domain **V** (C terminus, aa 408–519) of the β_4-subunit. 97% of the cells infected with the C terminus and 72% of the cells infected with the N terminus colocalized with synaptobrevin II and showed a punctate pattern (Table I). Thus, either N or C terminus alone is sufficient for colocalization with synaptobrevin II (Fig. 6, *a–f*). In contrast, a deletion construct lacking both the N and C termini (aa 50–407; domains **II–IV**), such as GFP alone, revealed a homogenous, cytosolic localization. 72% of these cells showed no synaptobrevin II colocalization (Fig. 6, *g–i*) (data summarized in Table I). The punctate staining pattern and its colocalization with synaptobrevin II indicates that the N and C termini of GFP-β_4 are sufficient for synaptic targeting.

To investigate the physiological role of GFP-β_4, we measured EPSCs in the whole cell, voltage clamp configuration from autaptic hippocampal neurons infected with GFP-β_4 and GFP-β_4(Δ50–407) and compared them with the EPSCs from noninfected neurons. As shown in Fig. 5, *c* and *d*, GFP-β_4(Δ50–407) assembled to form a functional Ca^{2+}-channel when expressed together with the α_{1A}- and $\alpha_2\delta$-subunit in HEK293 cells. The channel revealed inactivation properties comparable with the GFP-β_4 assembled channels and increased the whole cell peak current measured at +10 mV (α_{1A}, −48 ± 4 pA (n = 5); $\alpha_{1A}/\alpha_2\delta$/GFP-$\beta_4$(Δ50–407), −1715 ± 390 pA (n = 17)). Since GFP-β_4(Δ50–407) did not colocalize with synaptobrevin II, specific presynaptic effects on synaptic transmission should become obvious only in the presence of GFP-β_4, but not in the presence of GFP-β_4(Δ50–407). Recordings were performed in

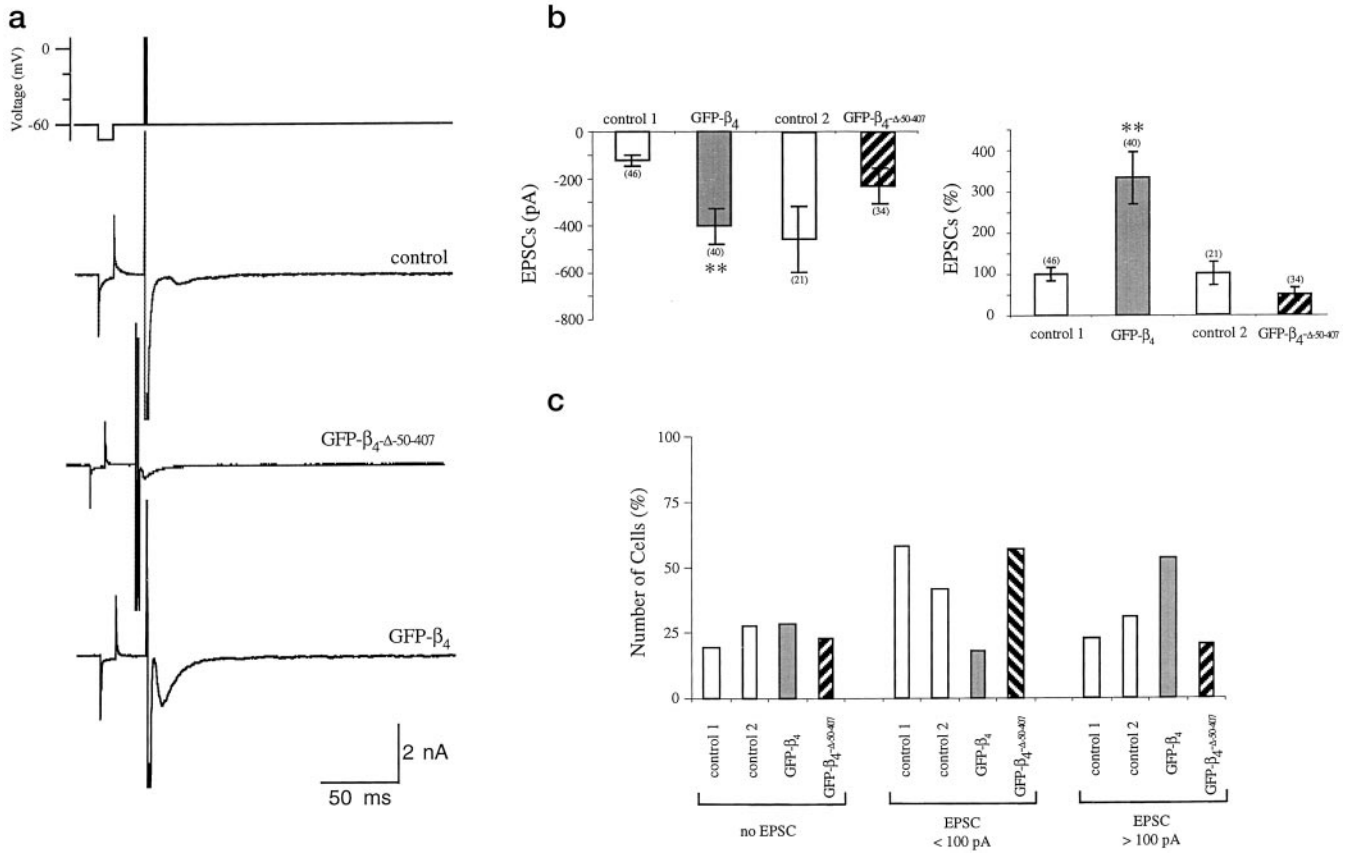

FIG. 7. **Effects of GFP-β_4 and GFP-β_4(Δ50–407) on EPSC amplitude of autaptic hippocampal neurons.** *a*, representative autaptic EPSC traces from noninfected neurons and infected GFP-β_4(Δ50–407) and GFP-β_4 neurons. EPSCs were elicited by a 2-ms depolarizing pulse to +10 mV. *b*, mean autaptic EPSC amplitude at 0.2 Hz stimulation in isolated hippocampal neurons. *Right*, EPSCs of infected neurons were compared with EPSCs of noninfected hippocampal cells (*control 1* and *control 2*) recorded from the same cell preparation. The average EPSC amplitude from GFP-β_4-infected neurons was significantly larger ($p < 0.01$; two-tailed *t* test) than noninfected neurons, whereas the average EPSC amplitude from GFP-β_4(Δ50–407) infected neurons was reduced compared with noninfected neurons. However, the effect was not significant. *Left*, EPSCs were related to the EPSCs of noninfected hippocampal cells recorded on the same day. *c*, number of EPSC measurements in hippocampal cells in percent for noninfected (control) and infected GFP-β_4 and GFP-β_4(Δ50–407) hippocampal neurons. Autaptic EPSCs recordings from hippocampal neurons were categorized in 3 groups: no EPSC could be detected, EPSC amplitudes smaller than 100 pA, and EPSC amplitudes larger than 100 pA. The diagram reveals that 58% (*control 1*) and 41% (*control 2*) of noninfected, 57% of GFP-β_4(Δ50–407)-infected, and only 18% of GFP-β_4-infected hippocampal neurons have EPSCs smaller than 100 pA, whereas 54% of GFP-β_4-infected hippocampal neurons and only 23% (*control 1*) and 31% (*control 2*) of noninfected and 21% of GFP-β_4(Δ50–407)-infected hippocampal neurons have EPSCs larger than 100 pA. Number of neurons examined: control 1 = 57; control 2 = 29; GFP-β_4 = 56; GFP-β_4(Δ50–407) = 44.

the presence of 30 μM Cs^{2+}, which reduces the EPSC amplitude by >90%,[2] to more easily detect changes in EPSC size and facilitation properties between infected and noninfected cells. EPSC amplitudes for infected cells were related to the average EPSC size measured for noninfected autaptic hippocampal neurons prepared and measured on the same day. The average EPSC size increased drastically from 100 ± 20% ($n = 46$) for noninfected neurons to 334 ± 63% ($n = 40$, $p < 0.01$) for GFP-β_4-infected neurons, but decreased for GFP-β_4(Δ50–407) infected neurons to 50 ± 17% ($n = 34$) (Fig. 7, *a* and *b*), indicating an increased transmitter release in the presence of GFP-β_4 but not GFP-β_4(Δ50–407).

Short term synaptic enhancements during repetitive synaptic activity are attributable to a presynaptic increase in the number of transmitter quanta released. Ca^{2+} entry during the conditioning stimulation is required for their induction (23, 24). We therefore analyzed the effects of GFP-β_4 and GFP-β_4(Δ50–407) on the facilitation properties of autaptic hippocampal neurons for EPSCs, which were larger than 80 pA and of comparable size in the infected and noninfected neurons. The ratios between the amplitudes of the first evoked EPSCs and the fourth evoked EPSCs for low and high frequency stimulations were determined. Low frequency stimulation (0.2 Hz) produced no EPSC facilitation in control (0.83 ± 0.04 ($n = 59$)), GFP-β_4-infected (0.86 ± 0.05 ($n = 33$)), or GFP-β_4(Δ50–407)-infected (0.92 ± 0.06 ($n = 24$)) cells (Fig. 8, *a* and *b*). In contrast, high frequency stimulation (20 Hz) led to paired pulse facilitation of EPSCs. More importantly, paired pulse facilitation is increased significantly from 1.47 ± 0.07 ($n = 44$) in control cells to 2.67 ± 0.29 ($n = 39$) in GFP-β_4-infected cells ($p < 0.01$) but not in GFP-β_4(Δ50–407)-infected cells (1.17 ± 0.06 ($n = 25$)) (Fig. 8, *c* and *d*), indicating a presynaptic function of GFP-β_4 on paired pulse facilitation.

To investigate whether the gating properties of a specific Ca^{2+}-channel type assembled with different β-subunits may account for the altered facilitation properties observed with overexpressed β_4-subunits in cultured hippocampal neurons, we analyzed Ca^{2+}-currents ($I_{Ca^{2+}}$) during high frequency stimulation of P/Q-type channels assembled with β_4 and β_{1b}. We transfected HEK293 cells with $\alpha_{1A}/\alpha_2\delta$ and β_4 or β_{1b}, respectively, and elicited $I_{Ca^{2+}}$ by a 20 Hz stimulation protocol. P/Q-type channels assembled with the β_{1b}-subunit inactivated faster (32.5 ± 2.1 ms ($n = 21$)) and to a higher degree (87 ± 2% ($n = 17$)) than channels assembled with the β_4-subunit (54.9 ± 7.5 ms ($n = 31$); 74 ± 2% ($n = 25$)) when 10-ms test pulses to +10 mV were applied (Fig. 9). 20 Hz application of 2-ms test pulses to +10 mV had no effect on the size of P/Q-type channel currents assembled with β_4, whereas $I_{Ca^{2+}}$ through β_{1b} assem-

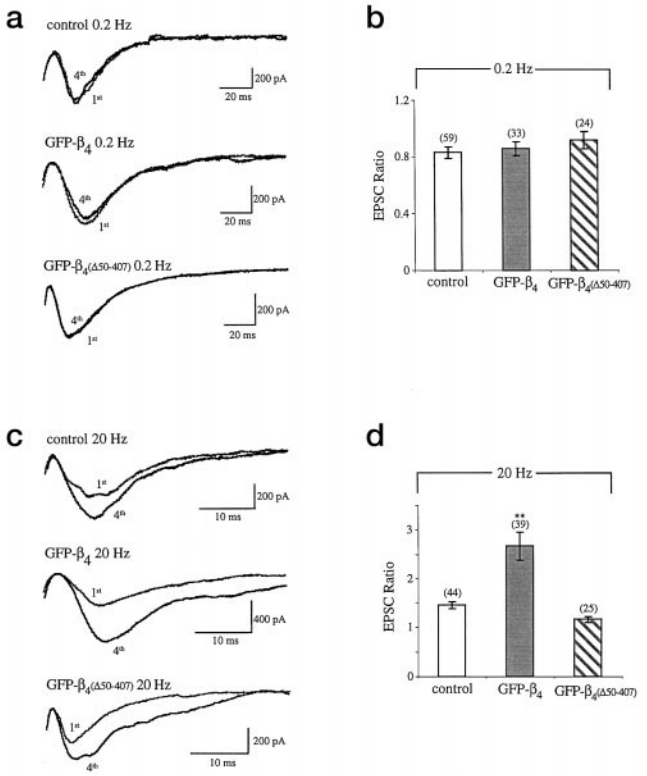

FIG. 8. **Effects of GFP-β_4 and GFP-β_4(Δ50–407) on paired pulse facilitation of autaptic hippocampal neurons.** *a*, representative autaptic EPSC traces from noninfected neurons (*control*) and neurons infected with GFP-β_4 or GFP-β_4(Δ50–407), respectively. 30 EPSCs were elicited at 0.2 Hz stimulation; the first and fourth EPSCs of one representative experiment are shown. *b*, EPSC ratios for 0.2 Hz stimulation are not significantly different between hippocampal neurons (*control*, *white bar*) and neurons infected with GFP-β_4 (*dark gray bar*) or GFP-β_4(Δ50–407) (*light gray bar*). *c*, representative autaptic EPSC traces from hippocampal neurons (*control*) and neurons infected with GFP-β_4 or GFP-β_4(Δ50–407), respectively. 30 EPSCs were elicited at 20 Hz stimulation and the first and fourth EPSCs of one representative experiment are shown. *d*, EPSC ratios for 20 Hz stimulation are significantly different between noninfected neurons (*control; white bar*) or GFP-β_4(Δ50–407) (*light gray bar*)- and GFP-β_4 (*dark gray bar*)-infected neurons ($p < 0.01$, two-tailed t test). EPSC ratios were calculated by dividing the amplitude of the first EPSC by the fourth EPSC within each set of experiment.

bled channels decreased slowly (249 ± 22 ms ($n = 20$) by 22.5 ± 1.8%) (Fig. 9). Thus, the assembly of P/Q-type Ca^{2+}-channel with different β-subunits at the presynapses may be responsible for the increased facilitation in the presence of overexpressed β_4.

DISCUSSION

In this study, we describe the synaptic distribution and function of the Ca^{2+}-channel β_4-subunit in cultured hippocampal neurons. Overexpression of a functional GFP-β_4 fusion protein in cultured hippocampal neurons revealed a punctate staining pattern similar to the distribution of synaptic proteins synapsin I, synaptophysin (25), Munc-13-1 (26), syntaphilin (18), and synaptobrevin (27, 28). Colocalization of GFP-β_4 with synaptobrevin II, a highly enriched presynaptic vesicle protein involved in transmitter release (29), and the presynaptic P/Q-type Ca^{2+}-channel α_{1A}-subunit suggests that GFP-β_4 is also targeted to the presynaptic terminals. The recent finding that α_{1A} and synaptobrevin are colocalized in mobile transport packets in hippocampal neurons (30) supports our results. Targeting signals to specific organelles have been identified in the extracellular and transmembrane domains of various proteins (31, 32). Infection of cultured hippocampal neurons with viral vectors is useful for identifying specific axonal sorting signals. For example, synaptobrevin contains a 92-aa long N-terminal region that is responsible for axonal targeting (28), whereas the metabotropic glutamate receptor 7 contains a 60-aa long cytoplasmic domain that mediates both axonal and dendritic targeting (33). To detect sequences responsible for targeting the β_4-subunit to presynaptic sites, we made use of the functional map and domain assignments suggested by Walker and De Waard (21) and Hanlon *et al.* (22). The identity of the N and C termini domains is only 2–3%, and these domains may therefore encode for different targeting signals among the β-subunits as suggested by the colocalization of the N and C termini GFP fusion constructs with synaptobrevin. In addition, a β_{1b}-specific acidic sequence in the C terminus has been described as responsible for membrane association of the β_{1b}-subunit (34). A comparison of the targeting sequences from the β_4-subunit and the presynaptically transported proteins synaptobrevin II and mGluR7 did not reveal any homology. Therefore, the N- and C-terminal targeting sequences of Ca^{2+}-channel β_4-subunit are distinct from other known presynaptic targeting signals. Interestingly, the C terminus of β_4 has been identified as a specifc, low affinity interaction site with the C terminus of α_{1A} (35). The specific interaction between α_{1A}- and β_4-subunits and the targeting to the presynapse mediated by β_4 may indicate how P/Q-type Ca^{2+}-channel complexes are assembled at the presynapse. However, the assembly of β_4-subunits with other α_1-subunits at the presynapse cannot be excluded.

Physiological studies point to a presynaptic function of the Ca^{2+}-channel β_4-subunit. For example, in lethargic mice where no functional β_4-subunit is expressed (36), the excitatory synaptic transmission in the thalamus and hippocampus, as well as the KCl-induced Ca^{2+}-uptake through P/Q-type channels in thalamic and neocortical synaptosomes, is reduced (37–39). In our study, we demonstrate a synaptic function of β_4-subunits in synaptic transmission because overexpression of GFP-β_4 but not GFP-β_4(Δ50–407) increased EPSC amplitude and paired pulse facilitation. One of the factors contributing to facilitation and EPSC size is the amount of Ca^{2+}-influx into the presynaptic terminal through voltage-gated Ca^{2+}-channels. β-subunits have been described as determining the transport of the pore-forming α_1-subunits to the cell surface and increasing the number of channels in the plasma membrane (3–7). An increase in the presynaptic Ca^{2+}-channel concentration may account for the larger EPSC amplitudes due to a higher release probability. We therefore measured somatic non-L-type Ca^{2+}-currents in GFP-β_4 infected and noninfected hippocampal neurons and observed a slight but not significant increase in current amplitude for GFP-β_4 infected cells (−0.748 ± 0.255 nA ($n = 9$)) compared with noninfected neurons (−0.446 ± 0.123 nA ($n = 9$)). Thus, other effects leading to an increase in EPSC amplitude and facilitation cannot be excluded. For example, if the Ca^{2+}-channel concentration at autaptic synapses does not change and the release probability at a single synapse is not affected by overexpression of β_4, then the successful transmission for a given action potential would remain unchanged. The formation of new synaptic contacts, new active sites, or postsynaptic effects, such as an increase in ligand gated cation channels, would explain our results. However, the altered facilitation properties point to a presynaptic mechanism.

The increase in the paired pulse facilitation ratio may reflect the slow inactivation time of presynaptic Ca^{2+}-channels assembled with the β_4-subunit for a limited access of Ca^{2+}, because β_4 causes Ca^{2+}-channels to inactivate slower compared with channel complexes containing β_{1b} or β_3 (19, 40). This hypothesis is underlined by our results showing that in the presence of β_4-subunits, inactivation is slower and current

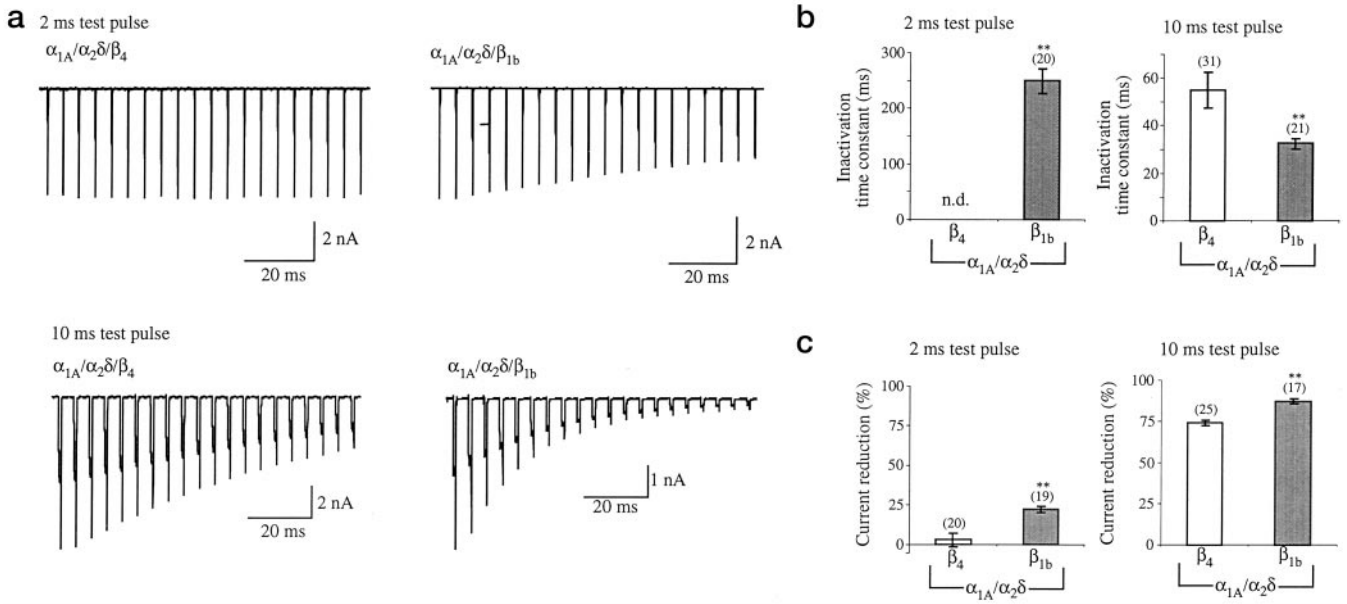

FIG. 9. **Effects of high frequency stimulation on P/Q-type Ca^{2+}-currents in HEK293 cells.** *a*, representative $I_{Ca^{2+}}$ traces from HEK293 cells transfected with α_{1A}, $\alpha_2\delta$, and β_4 (*left traces*) and α_{1A}, $\alpha_2\delta$, and β_{1b} (*right traces*). 20 tail currents were elicited by a 2-ms (*upper traces*) or 10-ms (*lower traces*) voltage pulse from −70 mV to +10 mV every 50 ms (20 Hz stimulation). *b*, inactivation time constants for P/Q-type channels assembled with β_{1b} or β_4 were determined by fitting the decreasing tail currents with a single exponential. Inactivation time constant for P/Q-type channels assembled with β_4 for the 2-ms test pulse could not be determined (*n.d.*) *c*, a larger reduction in $I_{Ca^{2+}}$ is evident with β_{1b}- compared with β_4-transfected cells following 2- and 10-ms test pulses. The percent current reduction was determined by comparing the size of the first elicited tail current and the last elicited tail current within the stimulation protocol.

reduction is decreased compared with P/Q-type channels expressed with β_{1b}. Therefore, Ca^{2+}-channel complexes containing β_4-subunits at the presynapse may contribute to increased synaptic facilitation.

In summary, our findings suggest a presynaptic function of Ca^{2+}-channel β_4-subunits in synaptic transmission. The specific targeting of β_4 depends on its nonconserved N and C termini, which is critical for the localization of the subunit to synaptic terminals and for the short term modulation of synaptic transmission.

Acknowledgments—We thank B. Rudo, A. Bührmann, and I. Herfort for excellent technical assistance. We are grateful to Drs. T. P. Snutch and E. Perez-Reyes for cDNAs, Dr. R. Jahn for the monoclonal antibody to synaptobrevin II, Dr. C. Rosenmund for helpful comments, and Drs. J. P. Ruppersberg and E. Neher for generous support.

REFERENCES

1. Catterall, W. A. (1998) *Cell Calcium* **24,** 307–323
2. Dunlap, K., Luebke, J. I., and Turner, T. J. (1995) *Trends Neurosci.* **18,** 89–98
3. Gregg, R. G., Messing, A., Strube, C., Beurg, M., Moss, R., Behan, M., Sukhareva, M., Haynes, S., Powell, J. A., Coronado, R., and Powers, P. A. (1996) *Proc. Natl. Acad. Sci. U. S. A.* **93,** 13961–13966
4. Yamaguchi, H., Hara, M., Strobeck, M., Fukasawa, K., Schwartz, A., and Varadi, G. (1998) *J. Biol. Chem.* **273,** 19348–19356
5. Gerster, U., Neuhuber, B., Groschner, K., Striessnig, J., and Flucher, B. E. (1999) *J. Physiol.* (*Lond.*) **517,** 353–368
6. Birnbaumer, L., Qin, N., Olcese, R., Tareilus, E., Platano, D., Costantin, J., and Stefani, E. (1998) *Bioenerg. Biomembr.* **30,** 357–375
7. Bichet, D., Cornet, V., Geib, S., Carlier, E., Volsen, S., Hoshi, T., Mori, Y., and M., D. W. (2000) *Neuron* **25,** 177–190
8. Ludwig, A., Flockerzi, V., and Hofmann, F. (1997) *J. Neurosci.* **17,** 1339–1349
9. Day, N. C., Volsen, S. G., McCormack, A. L., Craig, P. J., Smith, W., Beattie, R. E., Shaw, P. J., Ellis, S. B., Harpold, M. M., and Ince, P. G. (1998) *Brain Res. Mol. Brain Res.* **60,** 259–269
10. Volsen, S. G., Day, N. C., McCormack, A. L., Smith, W., Craig, P. J., Beattie, R. E., Smith, D., Ince, P. G., Shaw, P. J., Ellis, S. B., Mayne, N., Burnett, J. P., Gillespie, A., and Harpold, M. M. (1997) *Neuroscience* **80,** 161–174
11. Lie, A. A., Blumcke, I., Volsen, S. G., Wiestler, O. D., Elger, C. E., and Beck, H. (1999) *Neuroscience* **93,** 449–456
12. Jareb, M., and Banker, G. (1998) *Neuron* **20,** 855–867
13. Castellano, A., Wei, X., Birnbaumer, L., and Perez-Reyes, E. (1993) *J. Biol. Chem.* **268,** 12359–12366
14. Mark, M. D., Liu, Y., Wong, S. T., Hinds, T. R., and Storm, D. R. (1995) *J. Cell Biol.* **130,** 701–710
15. Herlitze, S., Garcia, D. E., Mackie, K., Hille, B., Scheuer, T., and Catterall, W. A. (1996) *Nature* **380,** 258–262
16. Bekkers, J. M., and Stevens, C. F. (1991) *Proc. Natl. Acad. Sci. U. S. A.* **88,** 7834–7838
17. Ashery, U., Betz, A., Xu, T., Brose, N., and Rettig, J. (1999) *Eur. J. Cell Biol.* **78,** 525–532
18. Lao, G., Scheuss, V., Gerwin, C. M., Su, Q., Mochida, S., Rettig, J., and Sheng, Z. H. (2000) *Neuron* **25,** 191–201
19. Stea, A., Tomlinson, W. J., Soong, T. W., Bourinet, E., Dubel, S. J., Vincent, S. R., and Snutch, T. P. (1994) *Proc. Natl. Acad. Sci. U. S. A.* **91,** 10576–10580
20. Westenbroek, R. E., Hoskins, L., and Catterall, W. A. (1998) *J. Neurosci.* **18,** 6319–6330
21. Walker, D., and De Waard, M. (1998) *Trends Neurosci.* **21,** 148–154
22. Hanlon, M. R., Berrow, N. S., Dolphin, A. C., and Wallace, B. A. (1999) *FEBS Lett.* **445,** 366–370
23. Fisher, S. A., Fischer, T. M., and Carew, T. J. (1997) *Trends Neurosci.* **20,** 170–177
24. Zucker, R. S. (1999) *Curr. Opin. Neurobiol.* **9,** 305–313
25. Fletcher, T. L., Cameron, P., De Camilli, P., and Banker, G. (1991) *J. Neurosci.* **11,** 1617–1626
26. Betz, A., Ashery, U., Rickmann, M., Augustin, I., Neher, E., Sudhof, T. C., Rettig, J., and Brose, N. (1998) *Neuron* **21,** 123–136
27. Li, J. Y., Edelmann, L., Jahn, R., and Dahlstrom, A. (1996) *J. Neurosci.* **16,** 137–147
28. West, A. E., Neve, R. L., and Buckley, K. M. (1997) *J. Cell Biol.* **139,** 917–927
29. Elferink, L. A., Trimble, W. S., and Scheller, R. H. (1989) *J. Biol. Chem.* **264,** 11061–11064
30. Ahmari, S. E., Buchanan, J., and Smith, S. J. (2000) *Nat. Neurosci.* **3,** 445–451
31. Keller, P., and Simons, K. (1997) *J. Cell Sci.* **110,** 3001–3009
32. Bradke, F., and Dotti, C. G. (1998) *Biochim. Biophys. Acta* **1404,** 245–258
33. Stowell, J. N., and Craig, A. M. (1999) *Neuron* **22,** 525–536
34. Bogdanov, Y., Brice, N. L., Canti, C., Page, K. M., Li, M., Volsen, S. G., and Dolphin, A. C. (2000) *Eur. J. Neurosci.* **12,** 894–902
35. Walker, D., Bichet, D., Campbell, K. P., and De Waard, M. (1998) *J. Biol. Chem.* **273,** 2361–2367
36. McEnery, M. W., Copeland, T. D., and Vance, C. L. (1998) *J. Biol. Chem.* **273,** 21435–21438
37. Caddick, S. J., Wang, C., Fletcher, C. F., Jenkins, N. A., Copeland, N. G., and Hosford, D. A. (1999) *J. Neurophysiol.* **81,** 2066–2074
38. Qian, J., and Noebels, J. L. (2000) *J. Neurosci.* **20,** 163–170
39. Lin, F., Barun, S., Lutz, C. M., Wang, Y., and Hosford, D. A. (1999) *Brain Res. Mol. Brain Res.* **71,** 1–10
40. Brody, D. L., and Yue, D. T. (2000) *J. Neurosci.* **20,** 889–898
41. De Waard, M., Pragnell, M., and Campbell, K. P. (1994) *Neuron* **13,** 495–503

MECHANISMS OF SIGNAL TRANSDUCTION:

Synaptic Localization and Presynaptic Function of Calcium Channel β_4-Subunits in Cultured Hippocampal Neurons

Silke Wittemann, Melanie D. Mark, Jens Rettig and Stefan Herlitze

J. Biol. Chem. 2000, 275:37807-37814.
doi: 10.1074/jbc.M004653200 originally published online August 7, 2000